Lattice dynamics in Bi_2Te_3 and Sb_2Te_3: Te and Sb density of phonon states

D. Bessas,[1,2] I. Sergueev,[1,3] H.-C. Wille,[4] J. Perßon,[1] D. Ebling,[5,*] and R. P. Hermann[1,2,†]

[1]*Jülich Centre for Neutron Science JCNS and Peter Grünberg Institut PGI, JARA-FIT, Forschungszentrum Jülich GmbH, D-52425 Jülich, Germany*

[2]*Faculté des Sciences, Université de Liège, B-4000 Liège, Belgium*

[3]*European Synchrotron Radiation Facility, F-38043 Grenoble, France*

[4]*Deutsches Elektronen-Synchrotron, D-22607 Hamburg, Germany*

[5]*Fraunhofer Institut Physikalische Messtechnik, Heidenhofstrasse 8, D-79110 Freiburg, Germany*

(Received 29 June 2012; revised manuscript received 10 September 2012; published 4 December 2012)

The lattice dynamics in Bi_2Te_3 and Sb_2Te_3 were investigated both microscopically and macroscopically using ^{121}Sb and ^{125}Te nuclear inelastic scattering, x-ray diffraction, and heat capacity measurements. In combination with earlier inelastic neutron scattering data, the element-specific density of phonon states was obtained for both compounds and phonon polarization analysis was carried out for Bi_2Te_3. A prominent peak in the Te specific density of phonon states at 13 meV, that involves mainly in-plane vibrations, is mostly unaffected upon substitution of Sb with Bi revealing vibrations with essentially Te character. A significant softening is observed for the density of vibrational states of Bi with respect to Sb, consistently with the mass homology relation in the long-wavelength limit. In order to explain the energy mismatch in the optical phonon region, a ∼20% force constant softening of the Sb-Te bond with respect to the Bi-Te bond is required. The reduced average speed of sound at 20 K in Bi_2Te_3, 1.75(1) km/s, compared to Sb_2Te_3, 1.85(4) km/s, is not only related to the larger mass density but also to a larger Debye level. The observed low lattice thermal conductivity at 295 K, 2.4 $Wm^{-1}K^{-1}$ for Sb_2Te_3 and 1.6 $Wm^{-1}K^{-1}$ for Bi_2Te_3, cannot be explained by anharmonicity alone given the rather modest Grüneisen parameters, 1.7(1) for Sb_2Te_3 and 1.5(1) for Bi_2Te_3, without accounting for the reduced speed of sound and more importantly the low acoustic cutoff energy.

DOI: 10.1103/PhysRevB.86.224301 PACS number(s): 63.20.dd, 76.80.+y, 72.20.Pa, 61.05.C−

I. INTRODUCTION

Binary pnictide chalcogenides with tetradymite crystal structure are semiconductors, with a typical band gap $E_g <$ 1 eV, and have been long studied mainly for potential thermoelectric applications as they exhibit a large thermoelectric figure of merit, $ZT \sim 1$, close to room temperature.[1] Recently, reversible phase switching from a crystalline to an amorphous phase induced by temperature or electric field[2,3] was reported. Because the phase change is accompanied by a large resistance change, such materials are considered candidates for future nonvolatile memory applications.[4] Furthermore, Bi_2Te_3 and Sb_2Te_3 as well as related compounds[5] are predicted to be three-dimensional topological insulators where the role of spin-orbit interaction[6] is important, and the topological insulator behavior of these materials has been experimentally established.[7,8] Lately, combined theoretical and experimental studies under extreme conditions were reported by Vilaplana *et al.*[9] on similar compounds pointing out the importance of lattice dynamics in this series of compounds.

Both Bi_2Te_3 and Sb_2Te_3 exhibit a layered rhombohedral lattice structure ($R\bar{3}m$, #160) with three quintuple -[Te(I)-Pn-Te(II)-Pn-Te(I)]- stacks, forming a unit cell, where Pn = Bi or Sb. The parenthetical indices, Te(I) and Te(II), denote two types of differently bonded tellurium atoms. Te(II) is coordinated nearly octahedrally by Pn atoms. In addition Te(I) has three Pn and three Te(I) as nearest neighbors and the coordination has not exactly octahedral geometry. The easy cleavage of these compounds perpendicular to the c axis is due to weak binding between the -Te(I)$\cdots$Te(I)- nearest neighbors.[10] The observed unit cell elongation, $c/a^{Bi_2Te_3} =$ 6.95, see room-temperature lattice parameters given in Table I, is indicative of a large structural anisotropy, which was reported also for the electrical properties.[11] Apart from transport anisotropy, layered compounds often also exhibit elastic anisotropy.

Several experimental techniques are specialized on the study of lattice dynamics.[12,13] However, access to the full density of phonon states (DPS) is feasible only by inelastic neutron[14] or x-ray scattering.[15] For most chalcogenides, due to structural complexity and formation of antisite defects, discussed, e.g., in Ref. 16, it is rather difficult to grow large single crystals for measuring phonon dispersion curves. Therefore we have studied the density of phonon states by nuclear resonant inelastic scattering, NIS. The NIS technique requires a Mössbauer active isotope and meV monochromatised synchrotron radiation of the corresponding nuclear resonant energy and provides the isotope specific, projected DPS.[17] Both Sb and Te have Mössbauer active isotopes, ^{121}Sb and ^{125}Te, respectively, however, no Bi Mössbauer active isotope exists.

Herein, we report both on the macroscopic characterization of Bi_2Te_3 and Sb_2Te_3 based on heat capacity measurements and on the microscopic characterization by synchrotron radiation diffraction and ^{121}Sb[18] and ^{125}Te[19] NIS. The combination of the Te DPS measured by NIS and the total DPS measured by inelastic neutron scattering[20] in Bi_2Te_3 allows us to obtain an approximative Bi DPS and to perform an elemental comparison for both compounds. Phonon polarization analysis was carried out on a Bi_2Te_3 single crystal measured with the incident radiation parallel and perpendicular to the c axis. Clues to the low thermal conductivity related to the acoustical cutoff and experimental insight on the difference in the nature

TABLE I. Refinement parameters (pseudohexagonal notation) for $Sb_2{}^{125}Te_3$ and $Bi_2{}^{125}Te_3$ at 295 K.

	$Sb_2{}^{125}Te_3$	$Bi_2{}^{125}Te_3$
Bragg R factor (%)	8.6	5.0
R_f (%)	10.6	4.5
a (Å)	4.2691(1)	4.3843(1)
	4.264(1)[a]	4.3835(3)[b]
c (Å)	30.4650(1)	30.4887(1)
	30.458(1)[a]	30.487(1)[b]
ρ (g/cm^3)	6.488(5)	7.857(5)

[a]Reference 23 for Sb_2Te_3.
[b]Reference 24 for Bi_2Te_3.

of the elemental binding between Bi_2Te_3 and Sb_2Te_3 are obtained.

II. EXPERIMENTAL METHOD

The nuclear inelastic signal for both Bi_2Te_3 and Sb_2Te_3 can be enhanced by enrichment with ^{125}Te. No further enrichment is required[21] for ^{121}Sb. The enriched samples were prepared by sealing stoichiometric amount of reactants, Sb or Bi and ^{125}Te metal with 95% enrichment, in a quartz tube under argon atmosphere and heated up to melting temperature. The sealed melt was then left to cool down under ambient conditions. The resulting amount was 50 mg of $Bi_2{}^{125}Te_3$ and 10 mg of $Sb_2{}^{125}Te_3$. Following the same procedure Bi_2Te_3 and Sb_2Te_3 with natural isotopic abundance were prepared.

Synchrotron radiation diffraction was performed at the 6-ID-D station of the Advanced Photon Source, at 295 K, on the isotopically enriched $Sb_2{}^{125}Te_3$ and $Bi_2{}^{125}Te_3$. The wavelength was 0.142519 Å. Data were collected using an amorphous Si area detector of 2048 × 2048 pixels (pixel size was 200 μm). The sample-detector distance of 1715.5 mm was refined by using diffraction from NIST Si 470c. The thermal expansion coefficient on the natural abundance Sb_2Te_3 and Bi_2Te_3 was measured using a calibrated Huber G670 image plate powder diffractometer.

The lattice dynamics were investigated by means of ^{121}Sb and ^{125}Te NIS using a backscattering sapphire single crystal monochromator[25] with a resolution of 1.1 and 1.3 meV for 35.49 keV ^{125}Te and 37.13 keV ^{121}Sb resonances, respectively. The spectra were recorded in 16-bunch mode at the nuclear resonance station ID22N[26] of the European Synchrotron Radiation Facility. The samples containing ∼10 mg of fine powder, evenly distributed on an area of 3 × 5 mm^2, were covered with aluminised mylar tape. In addition, for consistency check, similar measurements have been performed on a small nonenriched single crystal of Bi_2Te_3 from the same batch as in Ref. 27. Measurements on the single crystal carried out in two orientations, perpendicular and parallel to the crystallographic c axis. The obtained statistics were reduced compared to enriched polycrystalline samples but satisfactory to extract the DPS. Temperature-dependent measurements using ^{121}Sb and ^{125}Te NIS are not feasible due to the low Lamb-Mössbauer factor, see Table II and the related enhanced multiphonon contribution.[28] Thus, in order to minimize the multiphonon contribution, the measurements were carried out at 20 K. Heat capacity measurements on phase pure Bi_2Te_3 and Sb_2Te_3 were performed using the relaxation method of the Quantum Design (QD-PPMS) calorimeter between 3 and 300 K.

TABLE II. Summary of the lattice dynamics parameters, Lamb-Mössbauer factor f_{LM}, mean-square atomic displacement $\langle u^2\rangle$, and mean-force constants $\langle F_i\rangle$ obtained in this study at 20 K.

Compound	Method	f_{LM}	$\langle u^2\rangle$, 10^{-3}Å^{-2}	$\langle F_i\rangle$, N/m
Sb_2Te_3	^{125}Te NIS	0.53(1)	1.96(1)	61(2)
	^{121}Sb NIS	0.41(9)	2.52(1)	55(2)
Bi_2Te_3	^{125}Te NIS	0.52(1)	2.02(1)	58(2)
	"^{121}Bi" or ^{209}Bi	...	...	74(2)
Bi_2Te_3	^{125}Te NIS $k\|\|c$	0.54(1)	1.91(1)	68(3)
crystal	^{125}Te NIS $k \perp c$	0.52(1)	2.03(1)	58(3)

III. RESULTS

A. Microscopic characterization

X-ray diffraction on $Bi_2{}^{125}Te_3$, see Fig. 1, and on $Sb_2{}^{125}Te_3$, not shown, is indicative of a rhombohedral lattice, space group $R\bar{3}m$. The inset in Fig. 1 shows the Debye-Scherrer rings recorded using the area detector. No reflections from secondary phases are observed. In the same figure, the intensity distribution along the ϕ angle of the area detector is given. The (1 1 0), (0 1 5), and (0 0 15) reflections in the pseudohexagonal setting reveal a somewhat inhomogeneous azimuthal intensity distribution, which indicates slight preferential orientation. The preferred orientation was refined by the March-Dollase multiaxial function[29] with the assumption that the preferred orientation planes were the (1 1 0), (0 1 5), and (0 0 1 5). The

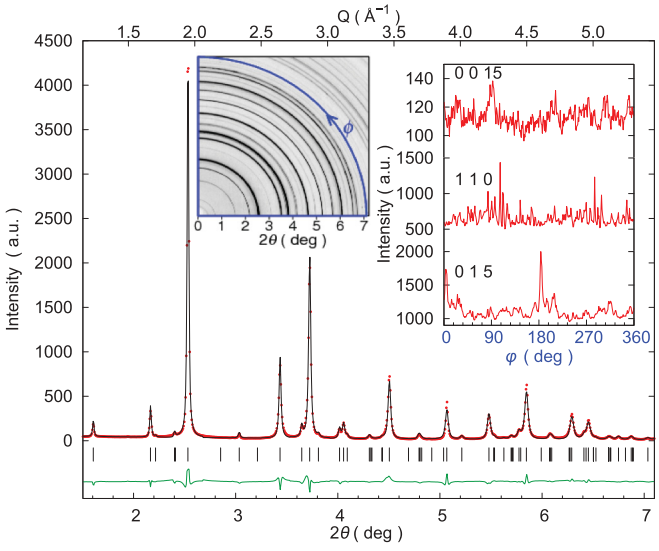

FIG. 1. (Color online) X-ray diffraction pattern of $Bi_2{}^{125}Te_3$ obtained at 295 K using synchrotron radiation (red dots), expected peak positions (black tics), corresponding refinement (black line) obtained using FULLPROF,[22] and difference plot (green line). (Inset) (Left) Quarter of the corresponding detector image and (right) intensity distribution along the ϕ angle for the (0 1 5), (1 1 0), and (0 0 15) reflections in the pseudohexagonal setting.

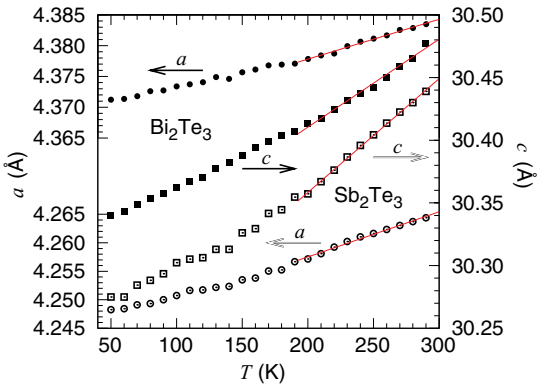

FIG. 2. (Color online) The temperature dependence of the a (circles) and c (squares) lattice parameters for Sb_2Te_3 (open tics) and Bi_2Te_3 (filled tics) between 50 and 300 K. Point sizes define error bar. The linear thermal expansion above 200 K in both orientations is indicated by red lines.

March-Dollase coefficients, r, that characterize the magnitude of the preferred orientation were 0.61, 0.68, and 1.69 respectively; random-oriented powder samples have $r = 1$. Moreover, the extracted r coefficient indicates that the (1 1 0) reflections have maximum pole density separated by 90° from the maximum pole density of the (0 0 15) reflections. This observation is expected for crystallites of the same symmetry. After the correction, the parameters obtained at 295 K are given in Table I. The lattice parameters of the ^{125}Te enriched samples appear increased by ∼0.1% with respect to nonenriched samples. However, within our instrumental resolution, $\frac{\Delta d}{d} \sim 5.0 \times 10^{-3}$, claims on the isotopic effects[30] in the unit-cell volume cannot be drawn. All in all, the lattice parameters obtained in this study are in good agreement with literature values.[23,24]

A temperature-dependent diffraction study on Bi_2Te_3 and Sb_2Te_3 was carried out for comparison and the refined lattice parameters are given in Fig. 2. Linear thermal expansion is observed between 200 and 300 K for both compounds. The volume thermal expansion coefficient, α_V, depends on the directional thermal expansion α_a and α_c by $\alpha_V = 2\alpha_a + \alpha_c$. The thermal expansion coefficients, α_a and α_c, were obtained from the derivative, $\alpha_a = [da(T)/dT]/a(300\ \mathrm{K})$, of the lattice parameter a and the corresponding expression for c. The extracted volume thermal expansion coefficient α_V of Bi_2Te_3 between 200 and 300 K is, $5.2 \times 10^{-5}\ \mathrm{K}^{-1}$, in excellent agreement with reference data.[31] For Sb_2Te_3, we obtain a volume thermal expansion coefficient, $\alpha_V = 7.1 \times 10^{-5}\ \mathrm{K}^{-1}$, in agreement with the previously measured[32] thermal expansivity.

The nuclear inelastic scattering spectra from ^{125}Te and ^{121}Sb in $Bi_2{}^{125}Te_3$ and $Sb_2{}^{125}Te_3$ together with the time integrated nuclear forward spectra, i.e., the instrumental function, are depicted in Fig. 3. In this work, the instrumental resolution was improved to 1.1 meV for ^{125}Te and 1.3 meV for ^{121}Sb with respect to 6.5 and 4.5 meV in the first demonstration of ^{125}Te and ^{121}Sb NIS,[18,19] respectively. After subtraction of the elastic peak, a modified version[33] of the program DOS[34] was used to extract the density of phonon states. The reliability of the procedure was verified using the conventional sum rules.[35] The

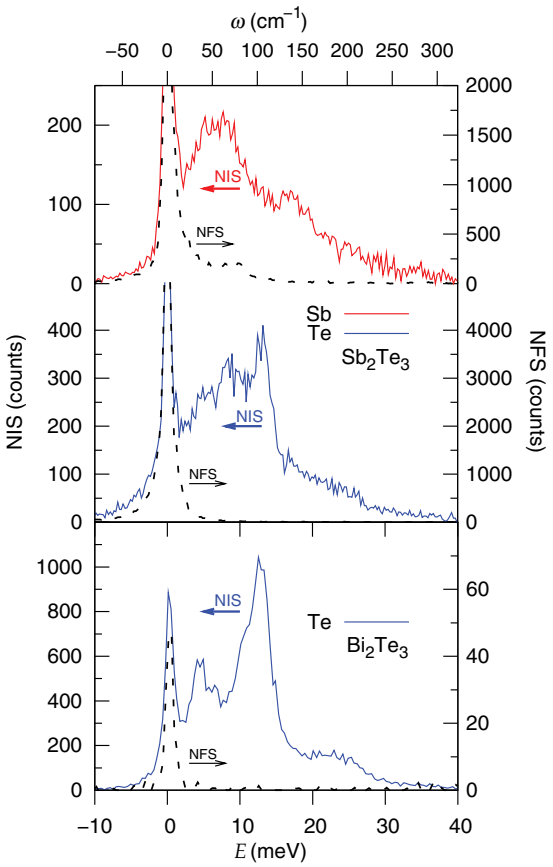

FIG. 3. (Color online) Nuclear inelastic scattering, NIS, spectra (lines) and the time integrated nuclear forward scattering, NFS-instrumental function, (dashed lines) obtained with the ^{125}Te (blue lines) and the ^{121}Sb (red line) resonances on $Bi_2{}^{125}Te_3$ and $Sb_2{}^{125}Te_3$.

obtained Sb and Te partial DPSs are shown in Fig. 5. A validity check was performed in Sb_2Te_3 where the partial Sb and Te DPSs were obtained by NIS and a total generalized DPS was measured by inelastic neutron scattering.[20] The agreement of the DPS measured using NIS at 20 K after neutron weighting[36] and the DPS measured using neutrons[20] at 77 K is substantial, see Fig. 4. In analogy, the procedure followed in extracting the Bi contribution in Bi_2Te_3 consists in subtracting the neutron weighted Te contribution measured using NIS on Bi_2Te_3 at 77 K from the total DPS measured using neutrons.[20] The obtained Bi DPS is shown in Fig. 5.

Phonon modes at the Γ point in Sb_2Te_3 have been calculated from first principles[37] and observed experimentally using Raman scattering measurements as well as IR spectroscopy.[38] The even g-modes are Raman active and odd u-modes are IR active. Color tics denote the main elemental contribution to the specific mode. Mode $E_u(3)$ and mode $A_{2u}(2)$ correspond to pure Te displacement. The displacement in the former is in the a-b plane the displacement in the latter is along the c axis. In contrast, the $A_{2u}(3)$ and $A_{1g}(2)$ modes are dominated by Sb displacements along the c axis. A signature of all Γ point phonon modes is visible in the DPS due to enhanced resolution, see Fig. 4.

In NIS, the absorption probability depends on the orientation of the incident radiation relative to atomic vibrations

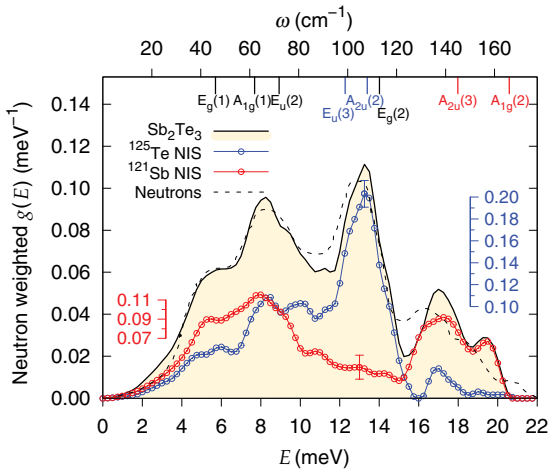

FIG. 4. (Color online) Density of phonon states measured with the ^{125}Te (blue points) and ^{121}Sb (red points) resonances at 20 K on Sb_2Te_3, for clarity a line is drawn between points and only one typical error bar is given. Comparison of the neutron weighted DPS[36] of Sb_2Te_3 obtained with NIS (highlighted area), see text, with the one obtained at 77 K using neutrons[20] (dashed line). Calculated[37] Γ-point phonon mode energies and symmetries are indicated by the labeled tics.

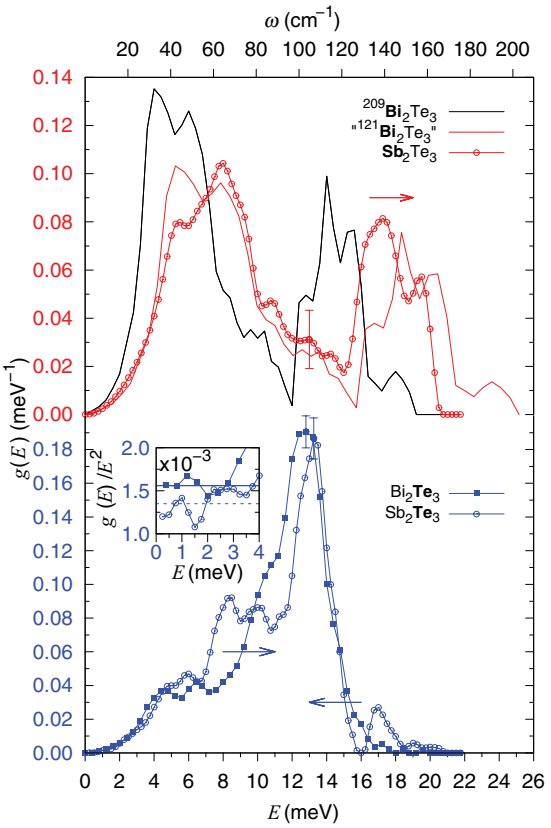

FIG. 5. (Color online) Element specific, Sb or Bi (in red) and Te (in blue), density of phonon states in Sb_2Te_3 (open circles) and Bi_2Te_3 (filled squares). The Bi specific DPS was extracted from the combination of NIS and reference neutron data[20] obtained at 77 K (black line) and renormalization according to a homology relation, see text, was applied (red line). (Inset) Debye level calculated from the Te specific DPS measured in Sb_2Te_3 and Bi_2Te_3.

and only the vibrational component along the incident beam is probed. Thus, in anisotropic crystal structures, provided that a single crystal is available, NIS is able to measure the different polarization of phonon modes.[39] Orientation-dependent measurements have been performed on a Bi_2Te_3 single crystal in two orientations, with the beam parallel and perpendicular to the crystallographic c axis and the extracted Te DPS in both cases is shown in Fig. 6. In case the incident beam is parallel to the c axis, a main peak around 14 meV arises in the Te DPS. This peak is identified as the $A_{2u}(2)$ phonon mode, which involves vibrations only along the c axis. When the incident beam is perpendicular to c axis, this $A_{2u}(2)$ mode does not appear in the Te DPS. Instead, a peak around 12.5 meV emerges and is identified as the $E_u(3)$ mode, which involves only in-plane atomic vibrations. The Debye level in both orientations is approximately equal, within 5%, and is shown as inset to Fig. 6. In addition, the first local minimum in the orientation dependent DPS is observed around 5(1) meV for radiation parallel and around 7(1) meV for radiation perpendicular to c axis. The isotropic DPS has been calculated from the directional dependent DPSs by averaging both contributions according to $DPS_{avg} = (2DPS_{k_{in}\perp c} + DPS_{k_{in}||c})/3$ and is shown in Fig. 6. Although the obtained statistics in the nonenriched single crystal were reduced the isotropic DPS extracted from such measurements is in very good agreement with the DPS extracted from polycrystalline sample.

NIS[40] is based on the Mössbauer effect and the probability of the recoiless absorption, known as Lamb-Mössbauer factor f_{LM} reveals the purely incoherent mean-square atomic displacement parameter, ADP, $\langle u^2\rangle = -\ln f_{LM}/k^2$, where k the wave number of the resonant photons. The extracted f_{LM} and ADP for both Te and Sb atoms as well as the Te orientation dependence in Bi_2Te_3 crystal are given in Table II.

From the DPS, a series of thermodynamical parameter are obtained from weighted integrals. The element specific Debye temperature is obtained directly from DPS using the expression $\theta_D^2 = 3/[k_B \int_0^\infty g(E)dE/E^2]$ valid in the high-temperature limit. The obtained Debye temperature for Te is 157(1) K for both compounds, significantly larger than 135(1) K obtained for Sb in Sb_2Te_3. The element specific mean-force constants $\langle F_i\rangle$ are obtained from the expression $\langle F_i\rangle = M_i \int_0^\infty g(E)E^2dE/\hbar^2$, where M_i is the mass of the resonant isotope. The obtained values are 61(1) N/m for ^{125}Te and 55(2) N/m for ^{121}Sb in $Sb_2{}^{125}Te_3$ and 58(1) N/m for ^{125}Te in $Bi_2{}^{125}Te_3$. In addition, the force constants parallel and perpendicular to the c axis extracted from similar measurements on a single crystal are given in Table II.The heat capacity at constant volume, $C_V(T)$, is also obtained from the total DPS using $C_V(T) = k_B \int_0^\infty g(E)\frac{(\beta E)^2\exp(\beta E)}{[\exp(\beta E)-1]^2}dE$, where $\beta = 1/k_BT$, in the rigid phonon approximation.[41] In Sb_2Te_3 where both Sb and Te contributions are available, the obtained C_V is given in Fig. 7.

The average speed of sound v_S was extracted from the ^{125}Te Debye level, $\lim_{E\to 0}\frac{g(E)}{E^2}$, shown in the inset of Fig. 5, using $\lim_{E\to 0}\frac{g(E)}{E^2} = \frac{M_i}{2\pi^2\hbar^3\rho v_S^3}$,[30] where ρ the mass density, and given in Table III.

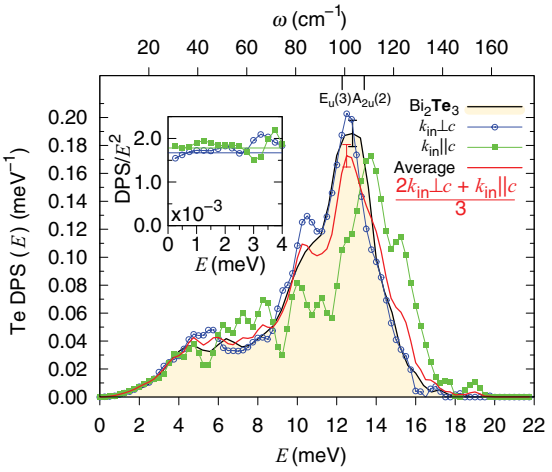

FIG. 6. (Color online) Orientation-dependent Te DPS measured on a Bi_2Te_3 single crystal parallel (green squares) and perpendicular (blue circles) to the crystallographic c axis. A comparison of the measured Te DPS in a Bi_2Te_3 polycrystalline sample (black curve) with the isotropic average obtained from data measured on single crystal (red curve) is given. (Inset) Debye level calculated in the two orientations (solid lines) from the measured Te specific DPS.

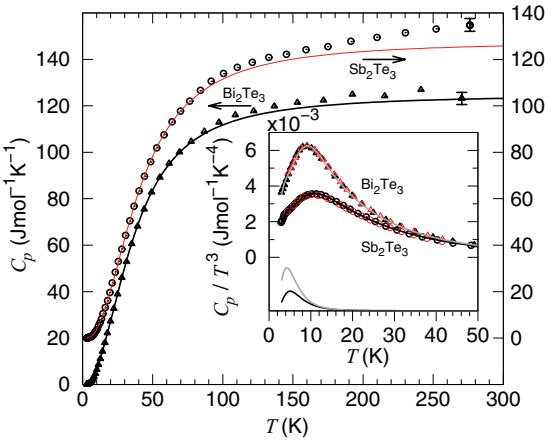

FIG. 7. (Color online) Specific heat at constant pressure C_P data measured on Sb_2Te_3 (circles) and Bi_2Te_3 (triangles) between 3 and 300 K and heat capacity at constant volume C_V calculated from low-temperature DPS (red line). A typical error bar is given. (Inset) the Debye representation C_P/T^3 of both measurements. A fit of the experimental data was applied using a two-level Schottky model superimposed to a Debye model with embedded Einstein oscillators (solid lines). The contribution of the Schottky model is given in the lower part of the inset. Specific heat measurements under 4−T magnetic field are shown as red symbols.

B. Macroscopic characterization

The measured specific heat at constant pressure, C_P, of natural isotope abundant Sb_2Te_3 and Bi_2Te_3 between 3 and 300 K is shown in Fig. 7. The obtained C_P in Bi_2Te_3 approaches smoothly the Dulong-Petit limit, 124.5 $Jmol^{-1}K^{-1}$ close to room temperature. In contrast, in Sb_2Te_3, the measured C_P deviates linearly from the Dulong-Petit limit between 230 and 300 K by 0.038 ± 0.009 $Jmol^{-1}K^{-2}$, indicating internal degrees of freedom related either to electronic properties or enhanced anharmonicity. In addition, a simple fitting of the measured C_P data in Sb_2Te_3 and Bi_2Te_3 with a model of a collection of Einstein oscillators embedded in a Debye solid gives Einstein temperatures around 55 K, see Table III, for both compounds. This model does, however, fail to reproduce adequately the experimental data below 30 K. We have modelled this deviation using a Schottky[42] model for a two level system. The contribution in the specific heat of a such two-level system is given by $C_S(\frac{\theta_S}{T})^2\exp(\frac{\theta_S}{T})/[1+\exp(\frac{\theta_S}{T})]^2$, where C_S is the Schottky heat capacity prefactor and θ_S is the Schottky temperature. After the introduction of these two additional free parameters a reduction of the reduced χ^2 from 462 to 3 was achieved. The resulting fit, between 3 and 80 K, as well as the Schottky contribution is shown in the inset to Fig. 7. The nature of the Schottky term was further investigated. In the literature, Schottky anomalies in the specific heat have been reported in paramagnetic salts[43] and heavy fermion systems[44] as well as in amorphous systems[45] and systems with artificially created defects.[46] In all cases, Schottky anomalies arise at low temperatures, moreover, in magnetic systems the related Schottky parameters have a magnetic field dependence.[47] Heat capacity measurements with a 4T applied magnetic field revealed no modification in heat capacity and no change in the Schottky contribution. The additional states concentration attributed to the Schottky term was calculated from the prefactor C_S given in Table III,

TABLE III. Summary of the thermodynamical parameters, speed of sound v_S, extracted from NIS at 20 K, Grüneisen parameter γ at 295 K, Debye temperature θ_D, Einstein temperature θ_E, Schottky temperature θ_S as well as the prefactors C_D, C_E, and C_S extracted from heat capacity measurements.

Compound	Method	v_S, km/s	γ	C_D, $Jmol^{-1}K^{-1}$	θ_D, K	C_E, $Jmol^{-1}K^{-1}$	θ_E, K	C_S, $Jmol^{-1}K^{-1}$	θ_S, K
Sb_2Te_3	^{125}Te NIS	1.90(2)	. . .	. . .	157(5)	. . .	. . .	. . .	. . .
	^{121}Sb NIS	. . .	. . .	. . .	135(5)	. . .	. . .	. . .	. . .
	Calorimetry	1.91(5)	1.7(1)	109(3)	179 (5)	18(1)	59(1)	0.9(1)	23 (1)
Bi_2Te_3	^{125}Te NIS	1.75(1)	. . .	. . .	157(5)	. . .	. . .	. . .	. . .
	Calorimetry	1.78(5)	1.5(1)	102(3)	164 (5)	23(1)	50(1)	1.2(1)	21 (1)
	Ultrasound	1.918[b]	. . .	. . .	165[a]	. . .	. . .	. . .	. . .
		1.394[b]	. . .	. . .	. . .	. . .	. . .	. . .	. . .

[a]Reference 23.
[b]From Ref. 23 using the Voigt and Reuss average[51] at 20 K.

with respect to the total thermodynamical degrees of freedom $C_D + C_E$. In Bi_2Te_3 the additional states amount to 0.9% and in $Sb_2{}^{125}Te_3$ to 0.6% of the total thermodynamical degrees of freedom.

IV. DISCUSSION

In this study, the calculated discrepancies between natural abundant Te, 127.60 amu, and our enriched ^{125}Te, 125 amu, according to the mass rule $\theta_D \sim M_i^{-1/2}$, where M_i is the isotopic mass, are in the range of experimental error, namely, 0.8%, and isotopic effects are neglected in what follows.

The Te projected DPS in Sb_2Te_3 and Bi_2Te_3 shown in Fig. 5, bottom, include a prominent peak, at 13 meV,which dominates the total DPS, and does not shift perceptibly upon substitution of Bi by Sb, which indicates pure Te vibrations. This was previously indirectly identified by a series of inelastic neutron experiments on powder samples[20] and shown in theoretical calculations.[23,37] Below 30 cm^{-1}, a minor discrepancy between the tellurium DPSs in Sb_2Te_3 and Bi_2Te_3 is observed and is related to the low-lying transverse acoustical phonons. Together with the increased mass density of Bi_2Te_3 with respect to Sb_2Te_3, see Table I, an 8% increase in the speed of sound in Sb_2Te_3 as compared to Bi_2Te_3 is obtained. Pronounced differences in the Te specific DPS between 7 and 13 meV, $E_u(2)$ modes, as well as between 17 and 19 meV, $A_{2u}(3)$ and $A_{1g}(2)$ modes, are seen in the two studied compounds. The aforementioned modes have contribution both from Sb and Te, as seen from the Fig. 5, and this might be the reason for the observed differences in the Te specific DPSs. In contrast, the comparison of the Sb and Bi DPSs reveal significant softening for the Bi compound, which is explained partly by the larger mass of the Bi atoms. Assuming the same electronic structure, a homology relation[48] can be applied to describe the mode energy difference $E_{Sb}/E_{Bi} = \sqrt{(M_{Bi}a_{Bi}^2)/(M_{Sb}a_{Sb}^2)}$. The mass ratio $\sqrt{M_{Bi}/M_{Sb}} = 1.66$ and the lattice constants ratio $a_{Bi}/a_{Sb} = 1.000$ or 1.027 for c and a, respectively, yield $E_{Sb}/E_{Bi} = 1.31$ or 1.35. The Bi DPS, scaled by 1.33 and renormalized to unity area is shown in Fig. 5, top, as "$^{121}Bi_2Te_3$." Such scaling is sufficient to describe the change in the low-energy part of the DPS. It is, however, too large to describe the change observed in the highest-energy optical part where a scaling factor of 1.25 would have to be used. This difference must be ascribed to a ~20% softening in force constant of Sb in Sb_2Te_3 as compared to Bi in Bi_2Te_3. The simultaneous stiffening of the low-energy acoustical phonons that results in increased speed of sound and the softening of the high-energy optical phonons that results in reduced force constants is a unique characteristic of phase change materials.[49] This behavior is observed here upon substitution of Bi with Sb and might be related to more favorable phase switching behavior in antimony than in bismuth bearing chalcogenides.[50] At the atomic scale, it might be related to the resonance bonding, which is highlighted in phase switching applications.[49] A similar effect in the DPS, i.e., rescaling of the high-energy optical phonons, might arise due to preferred orientation of the sample under investigation. However, the good correspondance of our measured element specific DPS using NIS with theoretical calculations as well as with reference data measured on polycrystalline material using neutrons preclude this explanation.

Macroscopic experimental techniques usually deal with integrals of microscopic quantities, among them, heat capacity measurements were used. From the low temperature data, see inset to Fig. 7, in Bi_2Te_3 and Sb_2Te_3 the extracted Debye and Schottky temperatures are shown in Table III. Although the Debye temperature depends on temperature, in the crude approximation of temperature independency the extracted value agrees within 15% with the value extracted from DPS in the high-temperature limit. Not surprisingly, the Debye temperature extracted from the Te specific DPS is the same for Bi_2Te_3 and Sb_2Te_3. The Schottky temperature is practically also the same in both compounds. Several explanations regarding this Schottky anomaly in heat capacity are possible. As the compounds have no magnetisation the magnetic origin should be discarded. Similarly, assuming that the origin of the Schottky term is of electronic nature, electronic spin polarization[52] is unlikely because no dependence on magnetic field was observed. A non spin-polarized electronic origin of the Schottky term can not be excluded *a priori*. The electronic contribution in heat capacity from activated charge carriers for semiconducting Bi_2Te_3 above 3 K is insignificant according to Shoemaker *et al.*[53] The presence of defects provides a plausible explanation as defect formation is an important issue in Bi_2Te_3. The energy scale for the existence of antisite defects has been recently calculated theoretically[16] and attemps to prove their existence experimentally[54] have been carried out. Activation of trapped charges around these antisite defects could contribute to the measured heat capacity as these charges will cause small lattice distortions. No irregularity is however observed around the expected energy, $E_{Schottky} = 1.8$ meV, in the measured DPS of both compounds. A reasonable explanation for this lacking observation is the low states concentration, below 1% in both cases, as well as the instrumental function of ~1 meV full width at half maximum, which hampers the observation of such small contribution that would be hidden in the tails of the elastic line. To the best of our knowledge, no direct relation of antisite defects in Bi_2Te_3 and Sb_2Te_3 with macroscopic physical properties have been reported so far. However, the relation of thermal properties with artificially created defects in crystalline materials has been extensively investigated. It was shown that presence of defects give rise to Schottky anomaly in heat capacity.[55] Similar behavior is observed in our heat capacity measurements. The two-level system was proposed to interact resonantly with thermal phonons leading to the T^2 dependence of thermal conductivity[56] below the temperature at which the peak in the Schottky term of heat capacity appears. Thermal conductivity data neither on Bi_2Te_3 nor on Sb_2Te_3 were found in literature at very low temperature, $T < 5$ K. In order to clarify the existence of resonant interaction of antisite defects with thermal phonons, we suggest that such thermal conductivity measurements below 5 K should be carried out.

Above 230 K, a strong deviation between the measured C_P and calculated C_V is observed only in Sb_2Te_3 whereas in Bi_2Te_3 C_P approaches the Dulong-Petit limit 124.5 Jmol^{-1}K^{-1} at 295 K. Similar effects were observed close to 300 K in previous calorimetric studies on Sb_2Te_3[57] with the temperature deviation between C_P and C_V being,

0.028 $Jmol^{-1}K^{-2}$, in agreement with our measurement. The band gap in Sb_2Te_3 and Bi_2Te_3 is $E_g \sim 0.1$ eV.[58] Thus the carrier activation temperature in both compounds is ~1000 K. At temperatures much lower than the corresponding carrier activation energies, anharmonicity effects are contributing in the specific heat expressed in the formula $C_P - C_V = \frac{a_V^2 V}{K_T} T$,[41] where K_T is the isothermal compressibility. Hence, our estimation of the Sb_2Te_3 isothermal compressibility between 230 and 300 K based on our C_P measurements and our C_V calculated from the total DPS is, $K_T = 1.3 \pm 0.3$ $Mbar^{-1}$, in quite poor agreement with the compressibility extracted from high pressure diffraction,[59] $K_T = 3.3$ $Mbar^{-1}$. Consequently, the observed deviation between C_P and C_V in Sb_2Te_3 might not have solely anharmonic origin. The excess in heat capacity close to room temperature in Sb_2Te_3 can possibly be attributed to electronic contribution due to self-doping, which has been highlighted in this compound.[60]

Macroscopic ultrasonic techniques which focus on the study of the speed of sound on either single crystal or polycrystalline materials are widely used.[61] In this study, we were not able to obtain a large macroscopically isotropic or single crystalline sample of Sb_2Te_3 and Bi_2Te_3. However, our microscopically extracted speed of sound can be directly compared to reference data on single crystals[23] using both the Voigt and Reuss averages.[51] With the Bi_2Te_3 mass density ρ of 7.86 g/cm^3 at 20 K the upper and lower limits in the speed of sound obtained from ultrasonic techniques on single crystals, i.e., related to isostress and isostrain conditions, are 1.918 and 1.394 km/s, respectively. The extracted speed of sound of this work is between the limits calculated from reference ultrasonic data. A second estimation of the speed of sound was obtained with the Debye approximation,[62] $v_S = k_B\theta_D/[\hbar(6\pi^2 N)^{1/3}]$, using our heat capacity measurements. The density of atoms for Bi_2Te_3 is 2.95×10^{22} $atoms/cm^3$ and for Sb_2Te_3 3.11×10^{22} $atoms/cm^3$. Hence using the Debye temperature extracted from our heat capacity measurements, the estimated speed of sound given in Table III is obtained. Not only is the speed of sound extracted from our macroscopic heat capacity measurements in excellent agreement with the one obtained from NIS but it also is largely smaller than in typical metallic systems, e.g., 3.750 km/s in Cu. Thus, in substances with layered structures, such as in Sb_2Te_3 and Bi_2Te_3, it seems that the shear modulus related with the first peak in the measured DPS dominates the long wavelength phonon propagation and results in reduced speed of sound.

Speed of sound and heat capacity are one constituent of thermal conductivity with the other being anharmonicity. The role of disorder and anharmonicity in the thermal conductivity have been thoroughly studied in the last years.[63] To quantify the anharmonicity in Bi_2Te_3 and Sb_2Te_3, the macroscopically extracted dimensionless Grüneisen parameter γ that is considered as a hallmark of anharmonicity was chosen. In this study, γ is defined by the formula $\gamma = \frac{\alpha_V}{C_V K_T}$ (see Ref. 42). In Bi_2Te_3, the Grüneisen parameter, using our measured volume expansivity, $a_V^{Bi_2Te_3} = 5.2 \times 10^{-5}$ K^{-1}, with hexagonal unit cell volume $V = 507$ $Å^3$, heat capacity under constant volume $C_V = 124.5$ $Jmol^{-1}K^{-1}$ and isothermal compressibility $K_T = 2.67$ $Mbar^{-1}$ (see Ref. 23) is $\gamma = 1.5(1)$ at 295 K. In Sb_2Te_3, from our measured expansivity, $a_V^{Sb_2Te_3} = 7.1 \times 10^{-5}$ $K^{-1}$of the hexagonal unit cell with volume $V = 481$ $Å^3$, at 295 K, heat capacity under constant volume $C_V = 124.5$ $Jmol^{-1}K^{-1}$ and isothermal compressibility $K_T = 3.3$ $Mbar^{-1}$ (see Ref. 59), the Grüneisen parameter is $\gamma = 1.7(1)$. Furthermore, in order to quantify anisotropic effects, the orientation dependent Grüneisen parameter has been extracted for Bi_2Te_3 by modifying the orientation dependent formulas given by Barron[64] for anisotropic crystal structure,[65] namely, $\gamma_a = [\alpha_a(c_{11} + c_{12}) + \alpha_c c_{13}]/C_V$ along the a direction and $\gamma_c = [\alpha_c c_{33} + 2\alpha_a c_{13}]/C_V$ along the c direction. The elastic constants c_{11}, c_{12}, c_{13}, and c_{33} at 280 K given by Ref. 23 are 0.685, 0.218, 0.270, and 0.477 Mbar, respectively. The direction-dependent thermal expansion measured herein in the same temperature range are $\alpha_a = 1.48 \times 10^{-5}$ K^{-1} and $\alpha_c = 2.30 \times 10^{-5}$ K^{-1}. In addition, close to room temperature, all phonon states in the DPS are populated, the heat capacity reaches the Dulong-Petit limit and can be considered isotropic. The estimated direction-dependent Grüneisen parameters along a, $\gamma_a = 1.6(1)$, and along c, $\gamma_c = 1.5(1)$, do not deviate significantly from the average Grüneisen parameter, $\gamma = 1.5(1)$. To elucidate the impact of the Grüneisen parameter on our measured DPS both in Bi_2Te_3 as well as in Sb_2Te_3, we used the vibrational energy defined Grüneisen parameter $\gamma = -\frac{d\ln E}{d\ln V}$. A straightforward way to change the unit cell volume is by conducting temperature-dependent studies. However, temperature-dependent ^{125}Te and ^{121}Sb NIS is not feasible above 100 K. The estimated phonon mode energy shift, between 50 and 100 K using our measured $\frac{\delta V}{V} \sim 0.005$ and our extracted average Grüneisen parameter of $\gamma = 1.6$ at 295 K results in $\frac{\delta E}{E} \sim 0.008$. Therefore even the highest energy phonon modes, around 20 meV, will not shift due to anharmonicity by more than 0.2 meV. Such energy mode shift is currently within the resolution limit for ^{125}Te and ^{121}Sb NIS. The small effect of anharmonicity on the DPS is also substantiated by the correspondence of our measured DPS on Sb_2Te_3 at 20 K and the DPS obtained by neutron scattering[20] at 77 K.

An empirical expression of the thermal conductivity in the umklapp scattering limit was derived by Toberer,[66] $\kappa_L = \frac{(6\pi^2)^{2/3}}{4\pi^2} \frac{\overline{M} v_S^3}{T V_{at}^{2/3} \gamma^2} (\frac{1}{N^{1/3}})$, where V_{at} is the volume per atom, $\overline{M}$ is the average atomic mass, and N is the number of atoms per primitive cell. Both Bi_2Te_3 and Sb_2Te_3 have five atoms per primitive unit cell. Bi_2Te_3 has an average atomic mass of 168.29 amu with 33.8 $Å^3$ atomic volume. Sb_2Te_3 has 124.64 amu average atomic mass and 32 $Å^3$ atomic volume. Accordingly, the lattice thermal conductivity in the umklapp limit for Bi_2Te_3 would be 4.76 $Wm^{-1}K^{-1}$ and for Sb_2Te_3 is 3.65 $Wm^{-1}K^{-1}$ in contrast to 1.6 and 2.4 $Wm^{-1}K^{-1}$ observed at room temperature for Bi_2Te_3 and Sb_2Te_3 (see Ref. 67), respectively. In our calculation, the lattice thermal conductivity was extracted at room temperature but we used our measured speed of sound at 20 K. The calculated thermal conductivity in the umklapp scattering limit is not only overestimated compared to the measured thermal conductivity but it also shows that Bi_2Te_3 should have larger conductivity than Sb_2Te_3. Thermal transport of optical branches is generally neglected.[68] Because the Grüneisen parameter was taken into account in our estimation anharmonicity effects fail, at least in first

approximation, to explain this deviation. The acoustic mode Debye temperature θ_a can be extracted from the calorimetry estimated Debye temperature θ_D^{cal}, using the relation $\theta_a = N^{-1/3}\theta_D^{cal}$.[69] The lattice thermal conductivity derived by Slack[70] is given by Eq. (1):

$$\kappa_L = A\frac{\overline{M}\theta_a^3 V_{at}^{1/3} N^{1/3}}{\gamma^2 T}, \quad (1)$$

where $A \approx 3.1 \times 10^{-6}$ is a collection of physical constants. In both compounds Eq. (1) yields a reduced thermal conductivity, namely, 3.76 $Wm^{-1}K^{-1}$ in Bi_2Te_3 and 2.76 $Wm^{-1}K^{-1}$ in Sb_2Te_3, but still lower in Sb_2Te_3 than in Bi_2Te_3. Assuming that the only channel in thermal conduction is realized through the acoustical phonons the acoustic cutoff can alternatively be estimated by our element specific DPS. In both compounds, the tellurium contribution in the DPS is relatively smooth and does not change significantly upon substitution of Bi with Sb. The pnictide contribution, see Fig. 5, top, is more structured and indicates that the acoustical cutoff is 6(1) and 8(1) meV, i.e., $\theta_a = 71$ and 94 K for Bi_2Te_3 and Sb_2Te_3, respectively. The thermal conductivity calculated using these acoustical cutoff θ_a obtained by DPS is, 1.6(2) W/m/K for Bi_2Te_3 and 2.0(2) W/m/K for Sb_2Te_3, in better agreement with reference data,[67] 1.6 and 2.4 W/m/K, respectively.

NIS on anisotropic single crystals measures the DPS of modes with vibrations along the incident beam. However, the phonon polarization and the phonon transport directions do not coincide. For example, in case $k_{in} \perp c$, there are three modes. One is longitudinal, transporting along the basal plane, and the other two are transversal, one transporting along the c axis and the other one in the basal plane. In case $k_{in}||c$, the probed vibrations, one longitudinal transporting along the c axis and two transversal modes transporting in the basal plane, have one transversal mode transported in the basal plane in common with the $k_{in} \perp c$ case. The orientational dependent thermal conductivity, or equivalently the acoustic cutoff energy, thus can not be directly obtained from our measured orientational dependent DPS. If the direction dependent acoustic cutoff energies were available from our measurements, the thermal conductivity ratio $\kappa_L^{k_{in}\perp c}/\kappa_L^{k_{in}||c}$ could be estimated using Eq. (1) and compared to reference data,[71] $\kappa_{L\perp c} = 1.73$ $Wm^{-1}K^{-1}$ and $\kappa_{L||c} = 0.64$ $Wm^{-1}K^{-1}$. The same holds for the composite speed of sound. Thus, in order to further clarify the orientational dependence of thermal conductivity, detailed theoretical investigation are needed.

V. CONCLUSION

Lattice dynamics measurements using nuclear inelastic scattering by ^{125}Te and ^{121}Sb show that the softening of the low energy modes likely has an influence on the thermal conductivity and thus favorably impacts the thermoelectric properties. Bi_2Te_3 is acoustically softer than Sb_2Te_3 mainly due to the mass ratio of Bi and Sb. Although the thermal expansion coefficient is highly anisotropic in both compounds, the calculated Grüneisen parameter in Bi_2Te_3 shows no directional dependence. An additional 20% force constant softening of the Sb-Te bond with respect to the Bi-Te bond is required to explain the observed phonon softening of the high-energy optical phonons of Sb_2Te_3 compared to Bi_2Te_3. It appears that for thermoelectrics, as was also suggested for phase change materials,[72] the role and type of the elemental binding should be carefully investigated. Low-temperature heat capacity measurements indicate the existence of antisite defects in both compounds and further thermal conductivity measurements should clarify their interaction with thermal phonons. Close to room temperature a substantial deviation of measured heat capacity from Dulong-Petit law is observed only in Sb_2Te_3 and attributed mainly to self-doping. We suggest that the low thermal conductivity observed in bulk tetradymite Pn_2Te_3 is essentially due to the low acoustic cutoff energy and the reduced speed of sound.

ACKNOWLEDGMENTS

The DFG priority program SPP1386 "Nanostructured Thermoelectrics" is acknowledged for the financial support of this study. R.H. acknowledges support from the Helmholtz–University Young Investigator Group "Lattice Dynamics in Emerging Functional Materials." RH and DB acknowledge the European Synchrotron Radiation Facility for provision of synchrotron radiation beam time and the helpful discussions with Dr. A. Chumakov and Dr. R. Rüffer during data acquisition at ID22N. Also the Advanced Photon Source for provision of synchrotron radiation beam time and the help of Dr. D. Robinson during data acquisition at 6-ID-D is acknowledged. We thank Dr T. Caillat and Dr. P. Fleurial for provision of the Bi_2Te_3 single crystal. We are grateful to Mr. M.Winkler and Dr. B. Klobes for helpful discussions and comments on the manuscript, respectively.

*Present address: Fachhochschule Düsseldorf, Universitätsstraße, D-40225 Düsseldorf, Germany.
†r.hermann@fz-juelich.de

[1] R. J. Mehta, Y. Zhang, C. Karthik, B. Singh, R. W. Siegel, T. Borca-Tasciuc, and G. Ramanath, Nat. Mater. **11**, 233 (2012).
[2] J. Liu, S. Liu, and J. Wei, Appl. Phys. Lett. **97**, 261903 (2010).
[3] N. Han, S. I. Kim, J.-D. Yang, K. Lee, H. Sohn, H.-M. So, C. W. Ahn, and K.-H. Yoo, Adv. Mater. **23**, 1871 (2011).
[4] M. H. R. Lankhorst, B. W. S. M. M. Ketelaars, and R. A. M. Wolters, Nat. Mater. **4**, 347 (2005).
[5] H. Zhang, C.-X. Liu, X.-L. Qi, X. Dai, Z. Fang, and S.-C. Zhang, Nat. Phys. **5**, 438 (2009).
[6] B.-T. Wang and P. Zhang, Appl. Phys. Lett. **100**, 082109 (2012).
[7] Y. Xia, D. Qian, D. Hsieh, L. Wray, A. Pal, H. Lin, A. Bansil, D. Grauer, Y. Hor, R. J. Cava *et al.*, Nat. Phys. **5**, 398 (2009).
[8] Y. L. Chen, J. G. Analytis, J.-H. Chu, Z. K. Liu, S.-K. Mo, X. L. Qi, H. J. Zhang, D. H. Lu, X. Dai, Z. Fang *et al.*, Science **325**, 178 (2009).
[9] R. Vilaplana *et al.*, Phys. Rev. B **84**, 104112 (2011).
[10] J. Drabble and C. Goodman, J. Phys. Chem. Solids **5**, 142 (1958).

[11] R. T. Delves, A. E. Bowley, D. W. Hazelden, and H. J. Goldsmid, Proc. Phys. Soc. London **78**, 838 (1961).

[12] P. Fornasini, J. Phys.: Condens. Matter **13**, 7859 (2001).

[13] A. S. Pine and G. Dresselhaus, Phys. Rev. B **4**, 356 (1971).

[14] M. Christensen, F. Juranyi, and B. B. Iversen, Physica B **385-386**, 505 (2006).

[15] E. Burkel, Rep. Prog. Phys. **63**, 171 (2000).

[16] A. Hashibon and C. Elsässer, Phys. Rev. B **84**, 144117 (2011).

[17] A. Chumakov and R. Rüffer, Hyperfine Interact. **113**, 59 (1998).

[18] H.-C. Wille, Y. V. Shvyd'ko, E. E. Alp, H. D. Rüter, O. Leupold, I. Sergueev, R. Rüffer, A. Barla, and J. P. Sanchez, Europhys. Lett. **74**, 170 (2006).

[19] H.-C. Wille, R. P. Hermann, I. Sergueev, U. Pelzer, A. Möchel, T. Claudio, J. Perßon, R. Rüffer, A. Said, and Y. V. Shvyd'ko, Europhys. Lett. **91**, 62001 (2010).

[20] H. Rauh, R. Geick, H. Kohler, N. Nucker, and N. Lehner, J. Phys. C **14**, 2705 (1981).

[21] The natural abundance of ^{121}Sb and ^{125}Te is 57% and 7%, respectively.

[22] Juan Rodríguez-Carvajal, Physica B **192**, 55 (1993).

[23] J. O. Jenkins, J. A. Rayne, and R. W. Ure, Phys. Rev. B **5**, 3171 (1972).

[24] T. L. Anderson and H. Krause, Acta Crystallogr. Sect. B **30**, 1307 (1974).

[25] I. Sergueev, H.-C. Wille, R. P. Hermann, D. Bessas, Y. V. Shvyd'ko, M. Zajac, and R. Rüffer, J. Synchrotron Radiat. **18**, 802 (2011).

[26] R. Rüffer and A. Chumakov, Hyperfine Interact. **97-98**, 589 (1996).

[27] *Handbook of Thermoelectrics*, edited by D. M. Rowe (CRC Press, 1995).

[28] A. I. Chumakov, A. Barla, R. Rüffer, J. Metge, H. F. Grünsteudel, H. Grünsteudel, J. Plessel, H. Winkelmann, and M. M. Abd-Elmeguid, Phys. Rev. B **58**, 254 (1998).

[29] C. J. Howard and E. H. Kisi, J. Appl. Crystallogr. **33**, 1434 (2000).

[30] M. Y. Hu, H. Sinn, A. Alatas, W. Sturhahn, E. E. Alp, H. C. Wille, Y. V. Shvyd'ko, J. P. Sutter, J. Bandaru, E. E. Haller *et al.*, Phys. Rev. B **67**, 113306 (2003).

[31] J. Barnes, J. Rayne, and R. U. Jr, Phys. Lett. A **46**, 317 (1974).

[32] X. Chen, H. D. Zhou, A. Kiswandhi, I. Miotkowski, Y. P. Chen, P. A. Sharma, A. L. L. Sharma, M. A. Hekmaty, D. Smirnov, and Z. Jiang, Appl. Phys. Lett. **99**, 261912 (2011).

[33] The DOS program was modified for reconvoluting the extracted DPS with a Gaussian function with the same FWHM as the measured time integrated NFS.

[34] V. Kohn and A. Chumakov, Hyperfine Interact. **125**, 205 (2000).

[35] H. J. Lipkin, Phys. Rev. B **52**, 10073 (1995).

[36] In order to compare the DPS acquired using nuclear inelastic spectroscopy and the corresponding using neutrons, the correct weighting factor should be applied. In first approximation, the neutron weighted DPS, $g_n(E)$ is given by $g_n(E) = \sum_i N_i g_i b_{c\,i}^2 / M_i$, where N_i is the number of atoms, $b_{c\,i}^2$ is the nucleus specific coherent neutron scattering length, and g_i is the element projected DPS.

[37] G. C. Sosso, S. Caravati, and M. Bernasconi, J. Phys.: Condens. Matter **21**, 095410 (2009).

[38] W. Richter and C. R. Becker, Phys. Status Solidi B **84**, 619 (1977).

[39] V. G. Kohn, A. I. Chumakov, and R. Rüffer, Phys. Rev. B **58**, 8437 (1998).

[40] R. Rüffer and A. Chumakov, Hyperfine Interact. **128**, 255 (2000).

[41] N. W. Ashcroft and N. D. Mermin, *Solid State Physics* (Brooks / Cole, 1976).

[42] E. S. R. Gopal, *Specific Heats at Low Temperatures* (Heynwood Books, 1966).

[43] R. Wielinga, J. Lubbers, and W. Huiskamp, Physica **37**, 375 (1967).

[44] R. Felten, F. Steglich, G. Weber, H. Rietschel, F. Gompf, B. Renker, and J. Beuers, Europhys. Lett. **2**, 323 (1986).

[45] W. A. Phillips, J. Low Temp. Phys. **7**, 351 (1972).

[46] J. W. Gardner and A. C. Anderson, Phys. Rev. B **23**, 474 (1981).

[47] R. Movshovich, A. Yatskar, M. F. Hundley, P. C. Canfield, and W. P. Beyermann, Phys. Rev. B **59**, R6601 (1999).

[48] H. R. Schober and W. Petry, *Lattice Vibrations* (Wiley-VCH Verlag GmbH, 2006).

[49] T. Matsunaga, N. Yamada, R. Kojima, S. Shamoto, M. Sato, H. Tanida, T. Uruga, S. Kohara, M. Takata, P. Zalden *et al.*, Adv. Funct. Mater. **21**, 2232 (2011).

[50] D. Lencer, M. Salinga, B. Grabowski, T. Hickel, J. Neugebauer, and M. Wuttig, Nat. Mater. **7**, 971 (2008).

[51] R. Hill, Proc. Phys. Soc. London, Sect. A **65**, 349 (1952).

[52] U. Heinzmann and J. H. Dil, J. Phys.: Condens. Matter **24**, 173001 (2012).

[53] G. E. Shoemake, J. A. Rayne, and R. W. Ure, Phys. Rev. **185**, 1046 (1969).

[54] N. Peranio, M. Winkler, Z. Aabdin, J. König, H. Böttner, and O. Eibl, Phys. Status Solidi A **521**, 163 (2012).

[55] M. Saint-Paul, J. C. Lasjaunias, and M. Locatelli, J. Phys. C **15**, 2375 (1982).

[56] Y. Wang, J. Phys. Chem. Solids **47**, 181 (1986).

[57] A. Pashinkin, A. Malkova, and M. Mikhailova, Russ. J. Phys. Chem. A **82**, 1035 (2008).

[58] B. Y. Yavorsky, N. F. Hinsche, I. Mertig, and P. Zahn, Phys. Rev. B **84**, 165208 (2011).

[59] N. Sakai, T. Kajiwara, K. Takemura, S. Minomura, and Y. Fujii, Solid State Commun. **40**, 1045 (1981).

[60] D. Hsieh, Y. Xia, D. Qian, L. Wray, J. H. Dil, F. Meier, J. Osterwalder, L. Patthey, J. G. Checkelsky, N. P. Ong *et al.*, Nature (London) **460**, 1101 (2009).

[61] A. Migliori and J. L. Sarrao, *Resonant Ultrasound Spectroscopy* (Wiley, 1997).

[62] R. P. Hermann, F. Grandjean, and G. J. Long, Am. J. Phys. **73**, 110 (2005).

[63] J. Garg, N. Bonini, B. Kozinsky, and N. Marzari, Phys. Rev. Lett. **106**, 045901 (2011).

[64] T. Barron, J. Collins, and G. White, Adv. Phys. **29**, 609 (1980).

[65] G. K. White, J. Phys. C **5**, 2731 (1972).

[66] E. S. Toberer, A. Zevalkink, and G. J. Snyder, J. Mater. Chem. **21**, 15843 (2011).

[67] D. Spitzer, J. Phys. Chem. Solids **31**, 19 (1970).

[68] B. Qiu and X. Ruan, Phys. Rev. B **80**, 165203 (2009).

[69] O. Anderson, J. Phys. Chem. Solids **12**, 41 (1959).

[70] G. A. Slack, Solid State Physics **34**, 1 (1979).

[71] A. Jacquot, N. Farag, M. Jaegle, M. Bobeth, J. Schmidt, D. Ebling, and H. Böttner, J. Electron. Mater. **39**, 1861 (2010).

[72] M. Wuttig and N. Yamada, Nat. Mater. **6**, 824 (2007).